Journal of Geodesy (1999) 73: 298–310

Journal of Geodesy

Geodetic measurement of horizontal strain across the Red River fault near Thac Ba, Vietnam, 1963–1994

Duong Chi Cong[1], **K. L. Feigl**[2]

[1] Institute of Geology, National Center for Natural Science and Technology, Nghia Do, Cau Giay, Ha Noi, Vietnam
e-mail: dccong@hotmail.com; Tel.: +84 4 8343 068; Fax: +84 4 8362 886
[2] UMR 5562, Centre National de la Recherche Scientifique, 14 av. Edouard Belin, 31400 Toulouse, France
e-mail: kurt.feigl@cnes.fr; Tel.: +33 5 61 33 29 40; Fax: +33 5 61 33 29 00

Received: 18 November 1997 / Accepted: 28 January 1999

Abstract. Geodetic measurements from 1963 through 1994 are used to estimate horizontal strain rates across the Red River fault near Thac Ba, Vietnam. Whether or not this fault system is currently active is a subject of some debate. By combining: (1) triangulation from 1963, (2) triangulation in 1983, and (3) Global Positioning System (GPS) observations in 1994, horizontal shear strain rates are estimated without imposing any prior information on fixed stations. The estimated rates of shear strain in ten triangular subnetworks surrounding the fault trace are not significantly different from zero at 95% confidence. The maximum rate of dextral shear is less than 0.3 μrad/year in all but one of the triangles. The estimates help bound the slip rate in a simple elastic dislocation model for a locked, vertical strike-slip fault. By assuming a locking depth of 5–20 km, the most likely values for the deep slip rate are between 1 and 5 mm/year of right-lateral motion. These values delimit the 23% confidence interval. At 95% confidence, the slip rate estimate falls between 7 mm/year of left-lateral motion and 15 mm/year of right-lateral motion.

Key words. Crustal deformation · triangulation · GPS

1 Introduction

As the southwest boundary of the south China block, the Red River fault plays an important role in the tectonics of Asia (Molnar and Tapponnier 1975; Tapponnier et al. 1982, 1990; Armijo et al. 1989). Over 900 km long, it accommodated 700 ± 200 km of left-lateral offset prior to the end of the Miocene (5 Ma) (Lacassin et al. 1993; Leloup et al. 1995). Since then, the fault appears to have changed sense, becoming right-lateral (Leloup et al. 1995). Although its trace is quite prominent in optical satellite images (Lacassin et al. 1994; Replumaz and Lacassin 1997), its present-day activity has not been precisely quantified. In its northwestern part, in Yunnan, China, the fault system includes two major strands in the Gasa valley (Leloup et al. 1995). One follows the base of the Ailao Shan (Mountains) while the other (“mid-valley”) strand crosses the valley floor. Here, Allen et al. (1984) estimate 3–7 mm/year of right-lateral slip, based on offset stream drainages and tenuous assumptions on their rate of incision. Trenching on the “mid-valley” strand leads to a most likely value of 2 mm/year and a possible range of 1–4 mm/year for the slip rate across the entire fault, using ^{14}C dating (Weldon et al. 1994). This measurement probably represents a lower bound for the total slip rate because the fault shows several traces in the pull-apart basin surrounding the trenching site.

At the continental scale, a kinematic quasi-rigid block model designed to minimize elastic strain energy predicts that the south China block moves 10 ± 5 mm/year at N110°E with respect to its southern neighbor Sundaland (Peltzer and Saucier 1996). This relative velocity implies 8.9 ± 4.5 mm/year of right-lateral strike-slip and 4.6 ± 2.3 mm/year of extension on the Vietnamese section of the Red River fault where it strikes N43°W (Fig. 1). The extensional component is a direct consequence of the fault geometry. Since the fault does not trace a small circle about the pole of relative rotation between the two blocks it bounds, the slip vector on the fault must include an oblique component which varies along strike (Briais et al. 1993; Peltzer and Saucier 1996).

Only two geodetic measurements pertain, albeit indirectly, to the Red River fault. The relative velocity of Shanghai, China, with respect to sites in Europe on the Eurasian plate, estimated by VLBI is 8 ± 0.5 mm/year in the direction N117 ± 4°E (Molnar and Gipson 1996). Since the line between these two benchmarks crosses several other actively deforming zones, the Very Long Baseline Interferometry (VLBI) velocity represents at

Correspondence to: K.L. Feigl

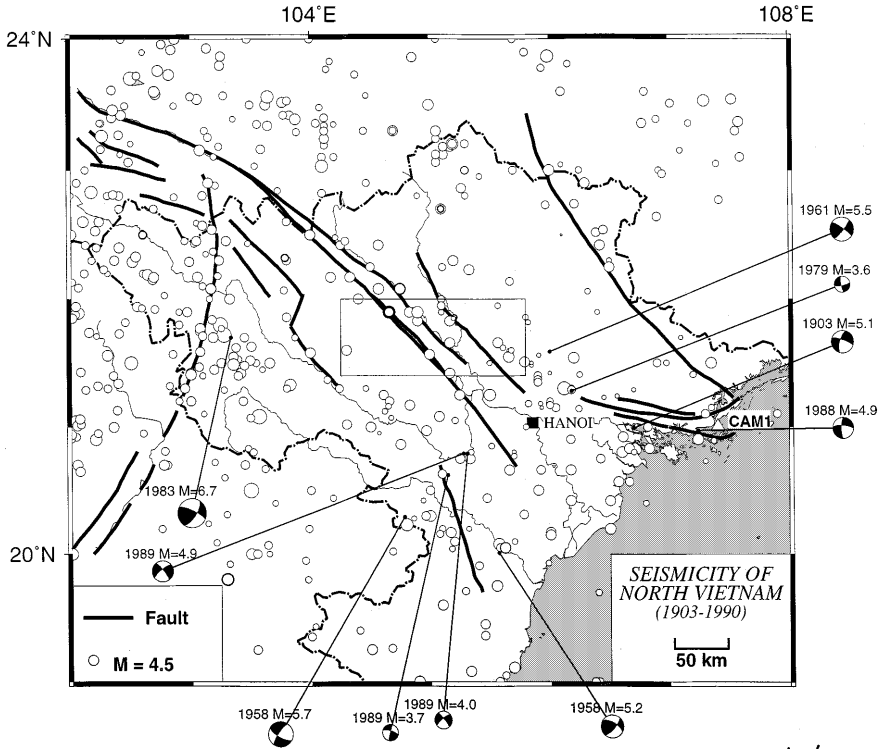

Fig. 1. Earthquake epicenters (*open circles*) of north Vietnam with magnitude $M > 1.0$ between 1903 and 1990 with several earthquake focal mechanisms based on "Geodynamic Seismicity of Vietnam", Hanoi Branch – Institute of Oceanography, NCNST, Hanoi, Vietnam, 1994 (in Vietnamese). *Heavy lines* Fault traces from Lacassin et al. (1994). *Rectangle* Delimits the study area shown in Fig. 2. *Open triangle* CAM1 station, one of two points in the GEODYSSEA network (Walpersdorf 1997). *Thin lines* Rivers; *dashed lines* international borders

best an upper bound for the slip rate of the Red River fault. Similarly, the relative velocity of benchmarks in Vietnam, Cam Pha (our station code CAM1) and Non Nuoc (NON4, near Da Nang), is 7.3 ± 3.1 mm/year at N161 ± 23°E based on Global Positioning System (GPS) measurements in 1994 and 1996 on the GEODYSSEA network (Walpersdorf 1997). The same author uses her geodetic velocities to estimate the rate of relative motion between two rigid plates: south China and Sundaland. The results of this model imply 13 mm/year right-lateral motion plus 12 mm/year of compression in the delta of the Red River, but uncertainties for these surprisingly rapid rates are not provided. Again, the long distance between the benchmarks prevents us from attributing all of this motion to the Red River fault alone.

The Red River fault shows relatively little instrumental seismicity. No earthquake with magnitude larger than 5.5 can be attributed to southern end of the fault in Vietnam between 1903 and 1990 (Fig. 1). Of course, this interval is considerably shorter than the recurrence time of a large earthquake, estimated to be 5000 to 7000 years (Weldon et al. 1994).

Clearly, the available data do not suffice to measure the present-day activity of the Red River fault system. In this

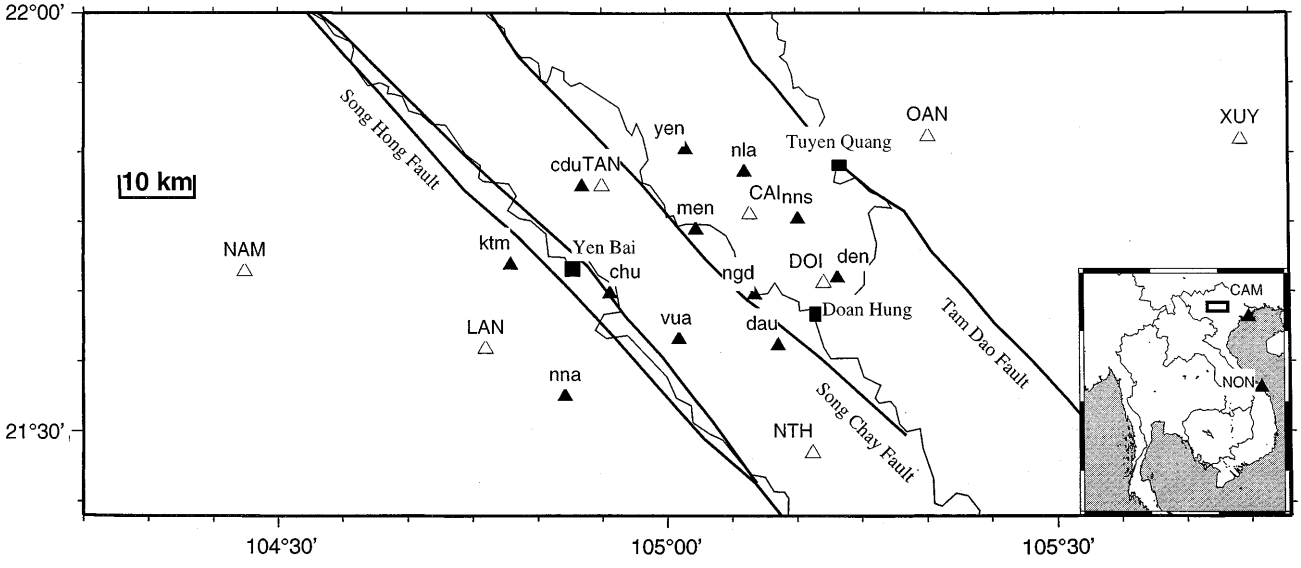

Fig. 2. Geodetic network with triangulation points (*solid triangles*), new GPS stations (*open triangles*), GEODYSSEA stations (*solid triangles* in inset map), provincial capital cities (*squares*), faults (*heavy lines*), and rivers (*thin lines*)

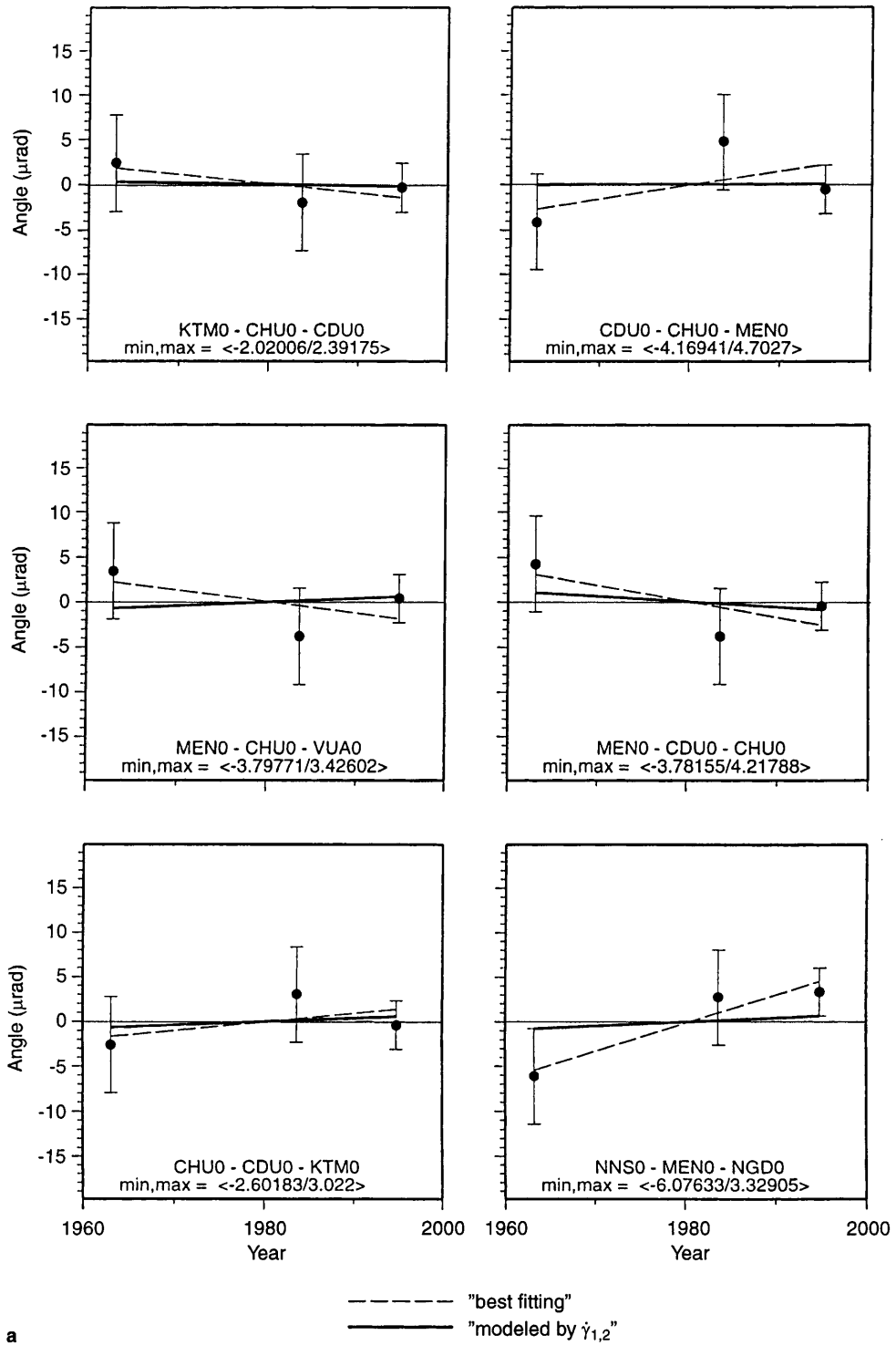

Fig. 3a–f. Measured angles α as a function of time, shown after subtracting their mean value α_0. *Min*, *Max* give the minimum and maximum values of $\alpha - \alpha_0$ in μrad. The *error bars* represent 1 SD on either side of the plotted angle. The *dashed line* is the "best fitting" line. The *solid line* shows the behavior predicted by $\dot{\gamma}_1$ and $\dot{\gamma}_2$. Nine angles are excluded from the data set: MEN0–NGD0–NNS0, CDU0–MEN0–NLA9, VUA0–CHU0–NNA9, and the six angles involving station DAU0

paper, we consider geodetic measurements in a fine-scale network spanning the fault zone over three decades. Specifically, the geodetic signature should distinguish between the following three competing hypotheses.

1. The fault is dead. Deformation in this area ceased sometime after the end of the Miocene (5 Ma).
2. The fault is active, but currently locked. In other words, the present day falls in an interseismic interval. The fault zone is accumulating strain as elastic potential energy to be released in a future earthquake.
3. The fault is actively releasing tectonic strain aseismically, presumably as creep, as documented in short (<100 km) segments of the San Andreas (Savage and Burford 1970) and Philippine (Duquesnoy et al. 1994) faults.

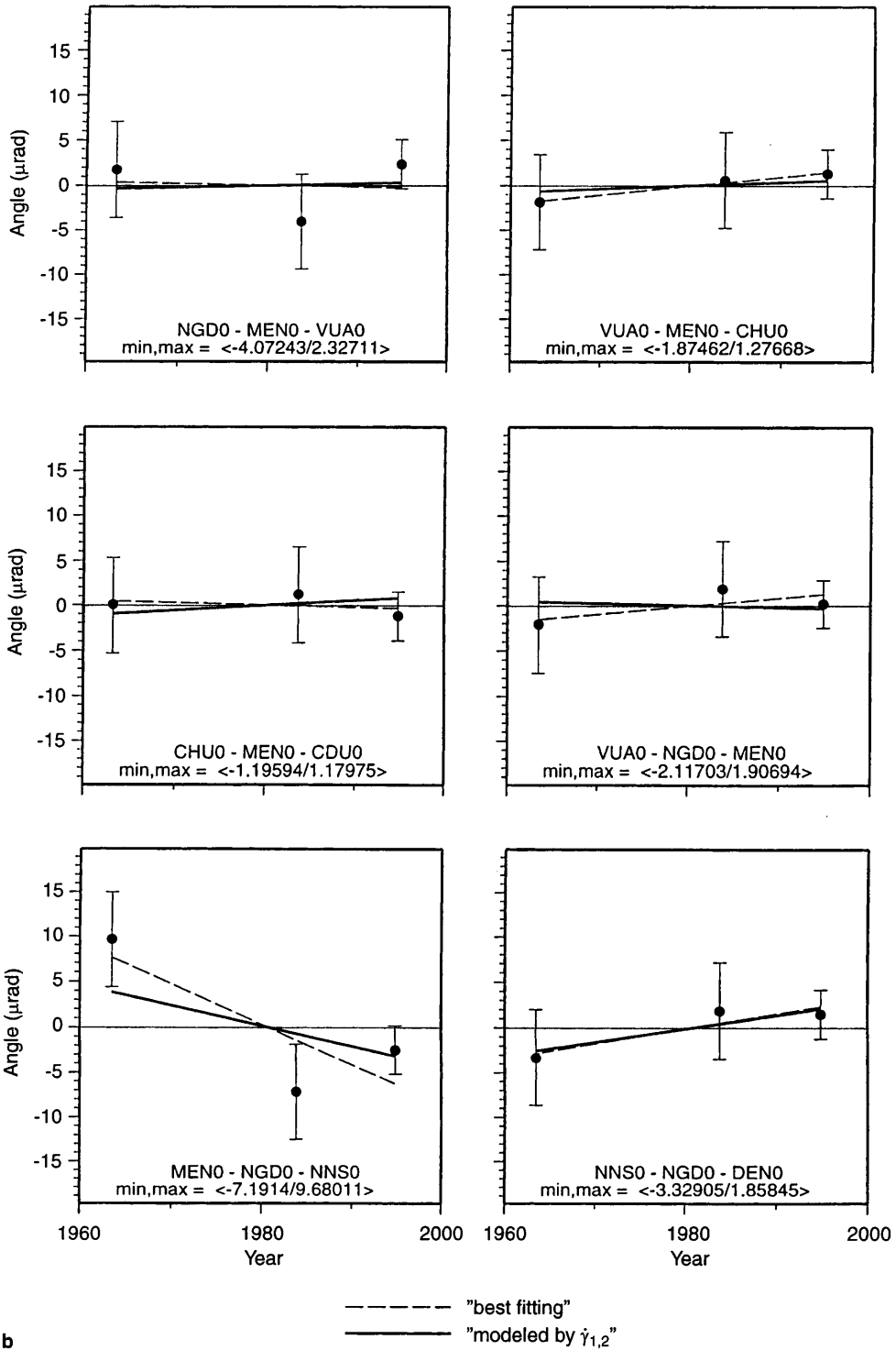

b

Fig. 3b

2 Data and precision

Our geodetic network in the study region consists of 20 stations, of which 12 are old triangulation points and 8 are new GPS benchmarks (Duong et al. 1994). In addition, we occupied two points in Vietnam of the continental-scale GEODYSSEA network described by Walpersdorf (1997) at Cam Pha and Non Nuoc (near Da Nang). The 12 triangulation and 8 new points span the Red River fault system in northern Vietnam. The network surrounds the Thac Ba reservoir and covers the provinces of Yen Bai, Tuyen Quang, Vinh Phuc, Phu Tho, and Bac Can (Fig. 2). Lacassin et al. (1994) have mapped three strands of the fault system using satellite images and field observations. From southwest to northeast, they are the Song Hong, Song Chay, and Tam Dao faults.

In 1963, during installation of the triangulation network for northern Vietnam, the 12 triangulation points were occupied with theodolites by the Geodetic Survey of Vietnam with the help of Chinese experts according to

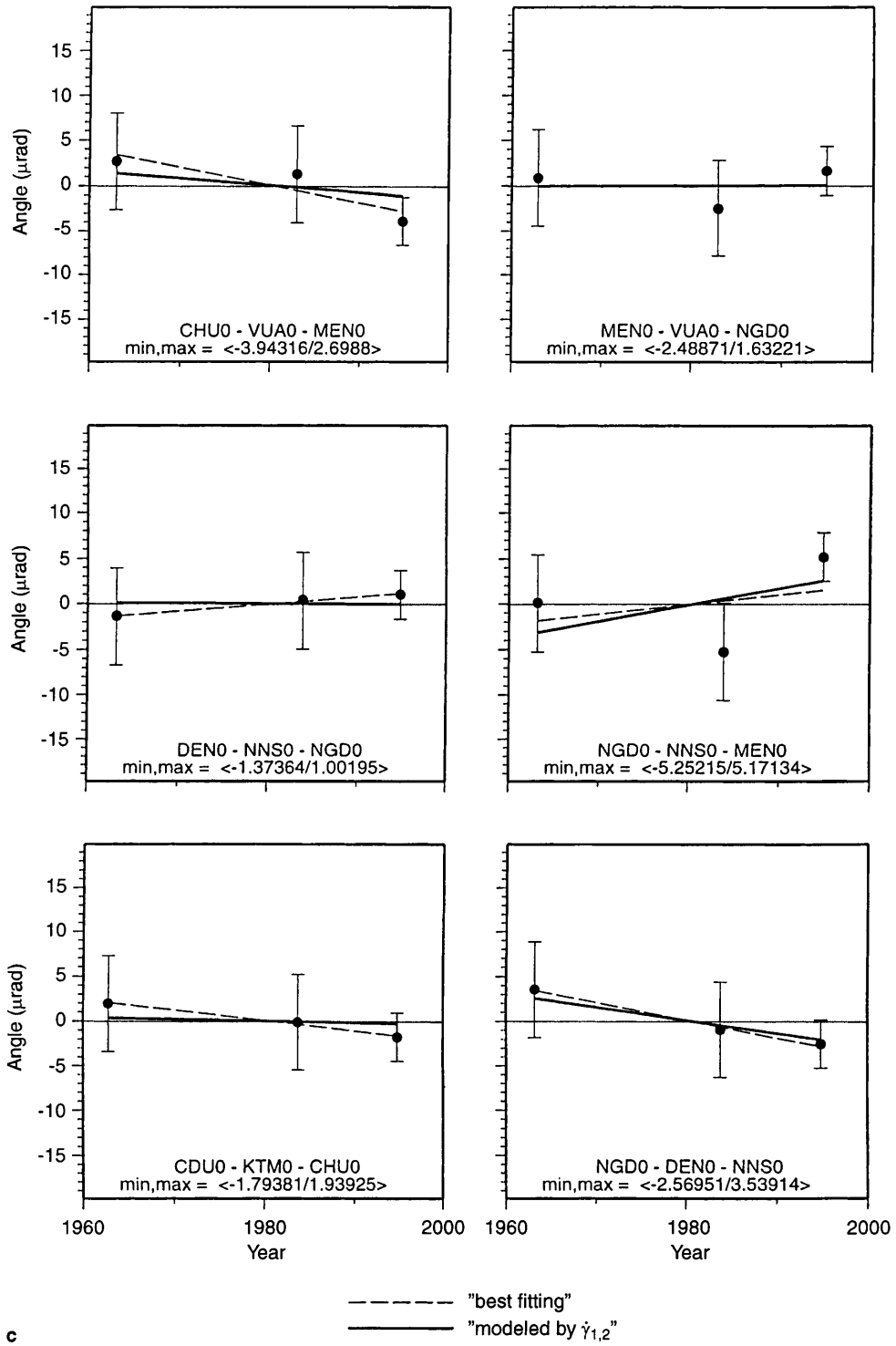

c

Fig. 3c

first- and second-order specifications. For this campaign, the data available to us are abstracted direction lists, that is, average values after "station adjustment" of 6 to 12 pointings.

In 1983 the same 12 triangulation points were measured a second time with theodolites according to first- and second-order specifications as part of the National Project on Recent Crustal Movements of the Red River delta (1981–1985). For this campaign, we have recovered the raw data for tie correction and deflection of the vertical. As for the 1963 survey, we have no data on atmospheric refraction. This time, four distances, averaging 13 km in length, were measured by trilateration with an average precision of ± 23 cm or 18 ppm. Because of this poor precision, we exclude these distances from our data set.

In order to assess the precision of the 1963 and 1983 triangulation measurements, we can employ two standard, but indirect approaches. First, we calculate misclosure in triangular subnetworks where all three angles

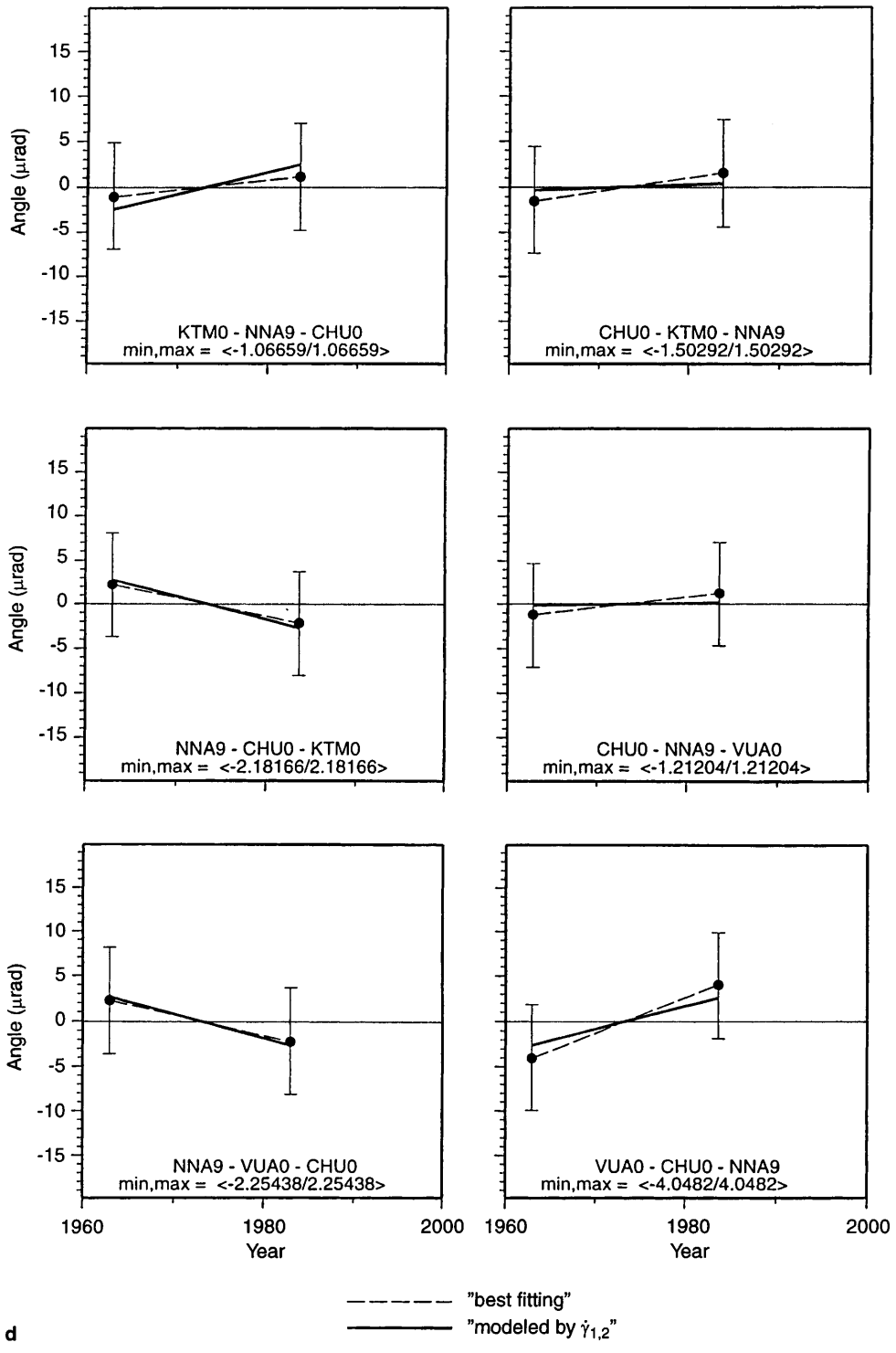

d

Fig. 3d

were observed, according to Ferrero's formula (Bomford 1980). Taking the 1963 and 1983 surveys together, we find the Ferrero misclosure to vary from a minimum of 0.02 arcsec to a maximum of 0.7 arcsec, and average 0.43 arcsec of arc. Secondly, the station adjustments (Bomford 1980) for the 1983 survey show that the standard deviation of a direction to varies between a minimum of 0.04 arcsec and a maximum of 0.68 arcsec, and averages 0.35 arcsec. Accordingly, we assign a value of 0.7 arcsec to the standard deviation (a priori uncertainty) of a single datum in our estimation procedure, in accord with the first-order specification.

GPS signals were recorded on all stations of our network from 22 October to 1 November 1994 using seven Ashtech receivers in an occupation strategy designed to maximize the network's sensitivity to the gradient of the displacement field generated by strain on the fault system.

We analyzed GPS observations using GAMIT software (King and Bock 1995) for the single-session solu-

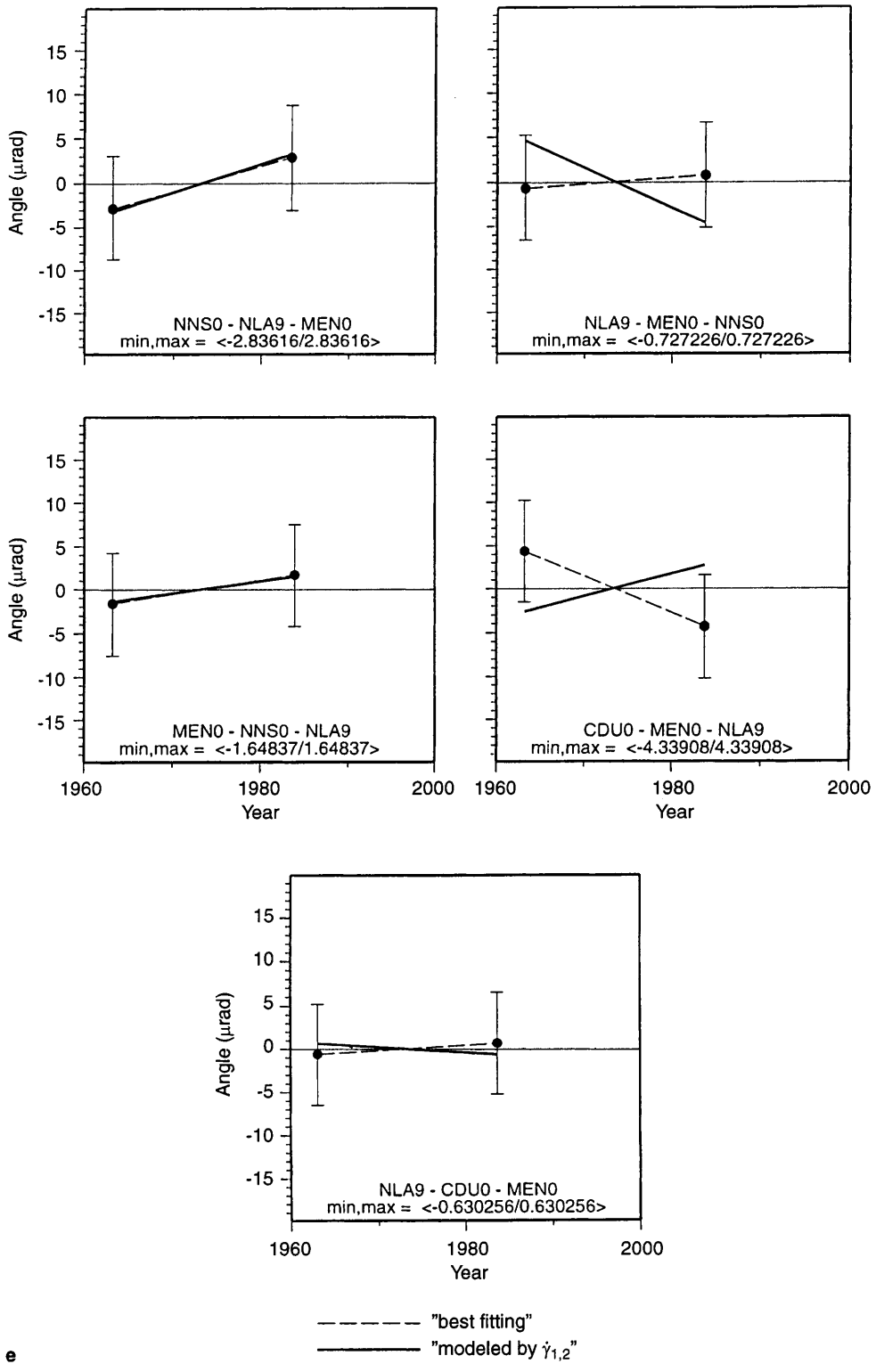

e

Fig. 3e

tions and GLOBK software (Herring 1995) to combine them according to standard procedures (Feigl et al. 1993), holding fixed the satellite orbital trajectories estimated by CODE (Beutler et al. 1994; Rothacher et al. 1996). We constrain the coordinates of station IISC (Bangalore, India) to its conventional ITRF94 coordinates (Boucher et al. 1996). The uncertainties range from 1 to 8 mm for the horizontal components, and from 8 to 114 mm for the vertical component as measured by the weighted root-mean-square (RMS) scatter. For the length, this precision depends on the distance between benchmarks as

$$\sigma_{\text{length}} = \sqrt{a^2 + (bL)^2} \tag{1}$$

where $a = 3.2\,\text{mm}$ and $b = 0.85 \times 10^{-6}$ for our results, and L is the distance between benchmarks.

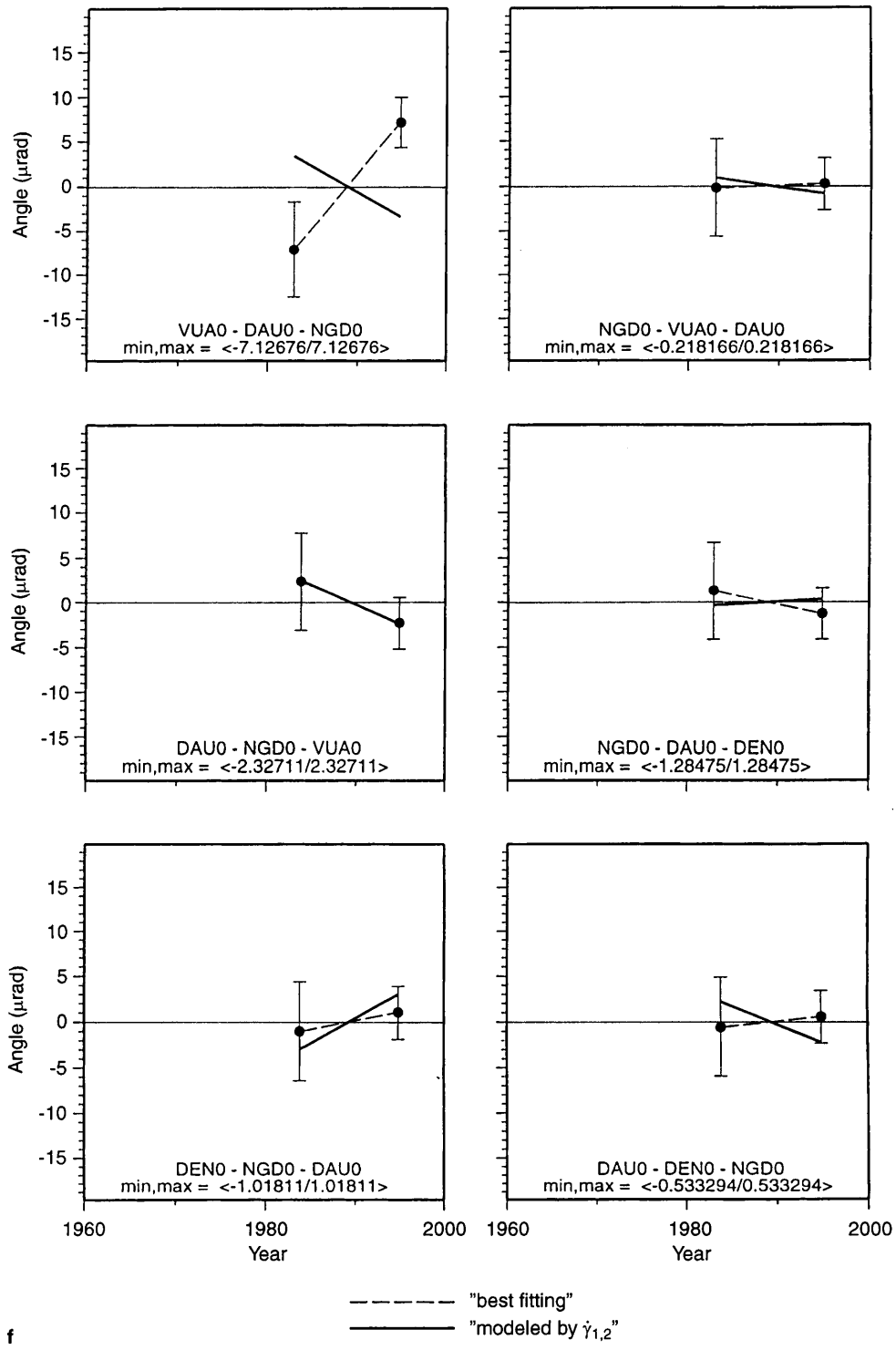

f

Fig. 3f

To adjust GPS measurements, we reduce them to direction lists on the ellipsoid almost as if they had been observed by theodolite. These we call "GPS ellipsoidal directions". Propagating errors through Eq. (1), we find the standard error of the mean for such a direction to be 0.2 arcsec.

The overall scaling factor for the standard deviations, as measured by the postfit normalized rms, is 0.68, 0.73, and 0.085 for the 1963, 1983, and 1994 adjustments, respectively. For the three-epoch adjustment, the value is 0.64. All four values satisfy the χ^2 test for the variance of unit weight (Vanícek and Krakiwsky 1986), validating our choice of data uncertainties. Consequently, we can say that there is no blunder in the triangulation measurements of 1963 and 1983. Furthermore, they and the "GPS ellipsoidal directions" are compatible.

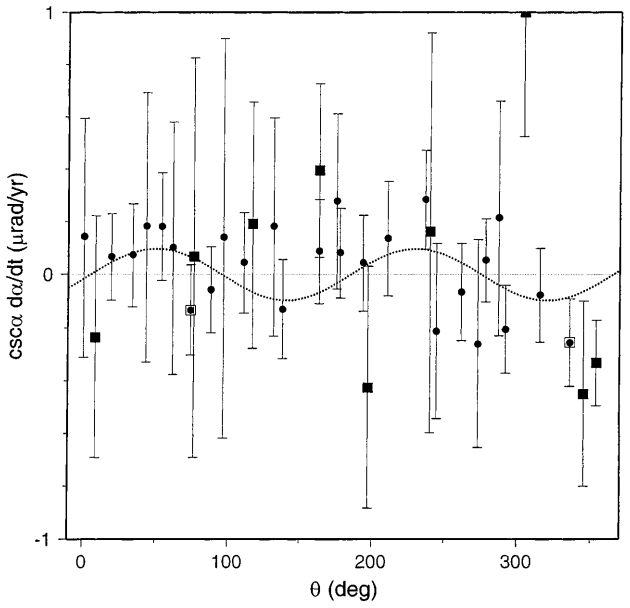

Fig. 4. Normalized angular rate of change $(\Delta\alpha_i/\Delta t_i)\text{cosec}\,\alpha_i$ as a function of bisector azimuth θ, measured clockwise from north, following Snay (1986). *Shaded circles* Angles included in the adjustment. *Open squares* Doubtful angles. *Solid squares* Angles excluded from data set. The *error bars* represent 1 SD of these normalized angular rates. The curve is calculated using the values of $\dot{\gamma}_1$ and $\dot{\gamma}_2$ estimated from the three-epoch 1963–1983–1994 data set for the whole network

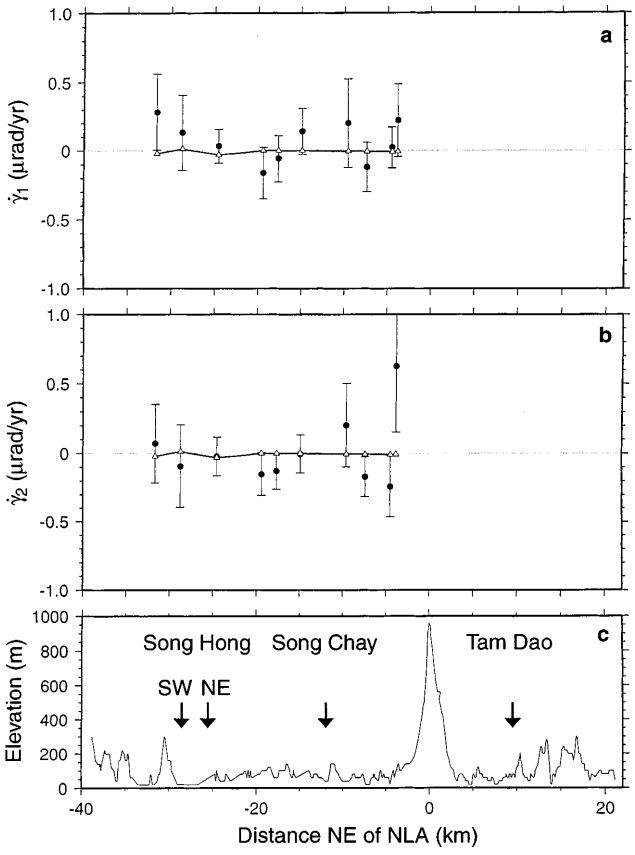

Fig. 5. Profile passing SW–NE through station NLA9 in the N45°E direction showing the angular shear strain rate parameters $\dot{\gamma}_1$ **a** and $\dot{\gamma}_2$ **b** respectively, and topographic relief taken from the 1:50 000 map **c**. The strain rates are plotted with *circular symbols* at the distance on the profile corresponding to the centroid of the Delaunay triangle in which they are estimated. The *heavy line* and *triangular symbols* in **a** and **b** indicate the values of $\dot{\gamma}_1$ and $\dot{\gamma}_2$ calculated from the most likely fault model. *Arrows* indicate where the named faults intersect the profile

3 Parameterization

From repeated geodetic measurements we can detect motion or estimate deformation parameters for a study area (Frank 1966; Prescott 1976; Bibby 1982; Feigl et al. 1990). Using the notation of Feigl et al. (1990) we can write the relative horizontal position (with respect to the spatial origin) of the mth station at time t_i as

$$\Delta x_i^{(m)} = \Delta x_0^{(m)} + (t_i - t_0)\mathbf{L}\Delta\xi_0^{(m)} \tag{2}$$

where $\mathbf{L}$ is the gradient of horizontal velocity (Malvern 1969) and $\xi_0^{(m)}$ is the preliminary value of coordinate of the mth station at time t_0. The components of $\mathbf{L}$ lead directly to the two engineering shear rates $\dot{\gamma}_1$ and $\dot{\gamma}_2$, the parameters we will interpret in terms of fault motion.

To define these parameters, we follow Jaeger and Cook (1979) and Snay (1986). Thus, $\dot{\gamma}_1$ measures the rate of change of a right angle between a ray pointed NW and one pointed NE. Similarly, $\dot{\gamma}_2$ corresponds to the rate of change of a right angle between a ray pointed E and one pointed S.

Neither $\dot{\gamma}_1$ or $\dot{\gamma}_2$ can distinguish between so-called pure and simple shear. For example, we expect $\dot{\gamma}_1 > 0$ for a right-lateral strike-slip fault striking NW, such as the Red River fault. For a visual interpretation of the other cases, see Fig. 5 of Feigl et al. (1990).

We will also use the maximum dextral shear rate, $\dot{\gamma}_{\max}$, defined as

$$\dot{\gamma}_{\max} = \sqrt{\dot{\gamma}_1^2 + \dot{\gamma}_2^2} \tag{3}$$

The azimuth ψ (clockwise from north) of the maximum shear rate is

$$\tfrac{1}{2}\arctan\,(\dot{\gamma}_1/\dot{\gamma}_2) \tag{4}$$

or

$$\tfrac{1}{2}\arctan\,(\dot{\gamma}_1/\dot{\gamma}_2) + \pi/2 \tag{5}$$

if the value of the second derivative of $\dot{\gamma}(\psi)$ from Malvern (1969) evaluated at $0.5\arctan\,(\dot{\gamma}_1/\dot{\gamma}_2)$ is less than, or greater than, zero, respectively. Equations (4) and (5) complete the formulas in Prescott et al. (1979) and Snay (1986).

Figure 3 shows the measured angles as a function of time. We show two lines on these plots. First, the dashed line shows the "best fitting" linear trend. Second, the solid line shows the behavior predicted by $\dot{\gamma}_1$ and $\dot{\gamma}_2$, as from Snay (1986).

For 18 of the 35 angles in our network, these two lines show the same trend. The apparent change in angle at site YEN is enormous, so we exclude these angles from our data set even though this site was measured three times.

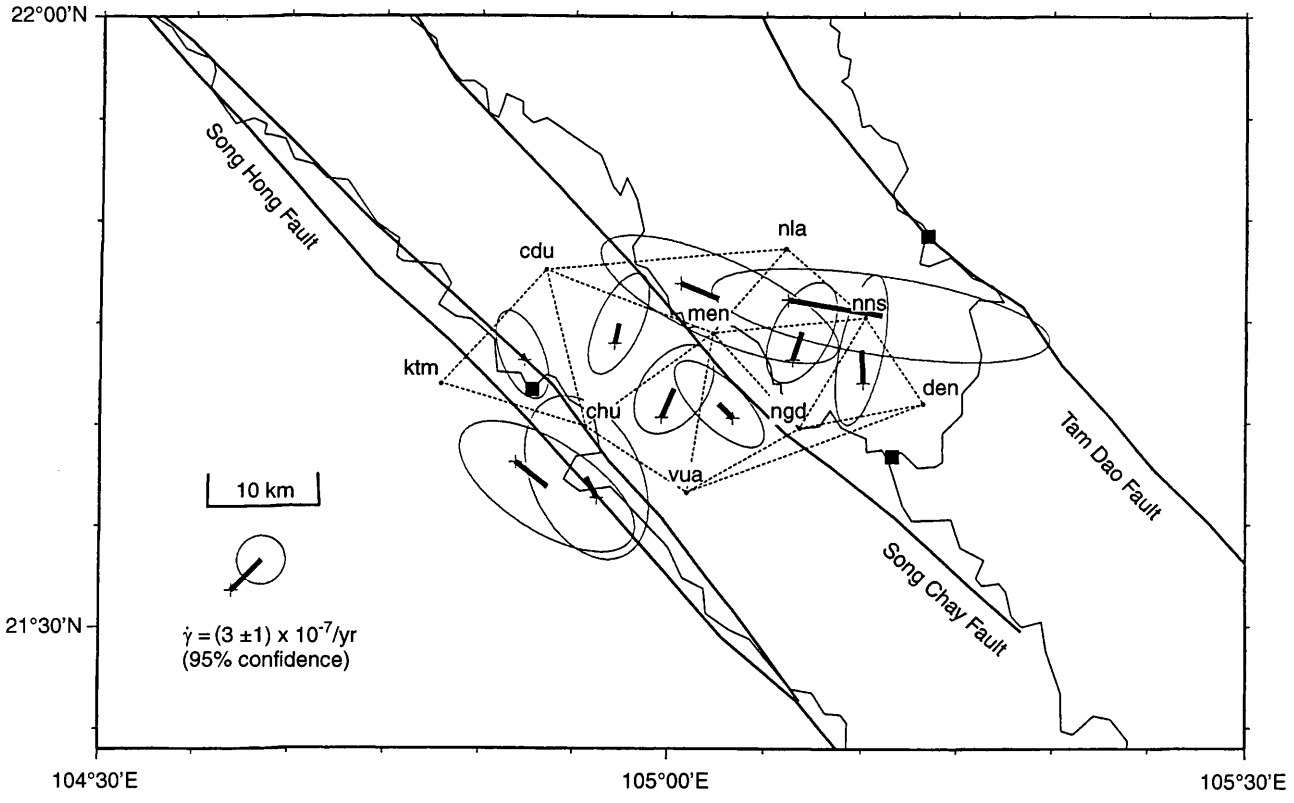

Fig. 6. Total (maximum) shear rate estimates over Delaunay triangles. *Crosses* include the centroid of a triangle and the origin of no deformation. *Error ellipses* represent 95% confidence intervals. *Squares* indicate the same cities as labeled in **Fig. 2**

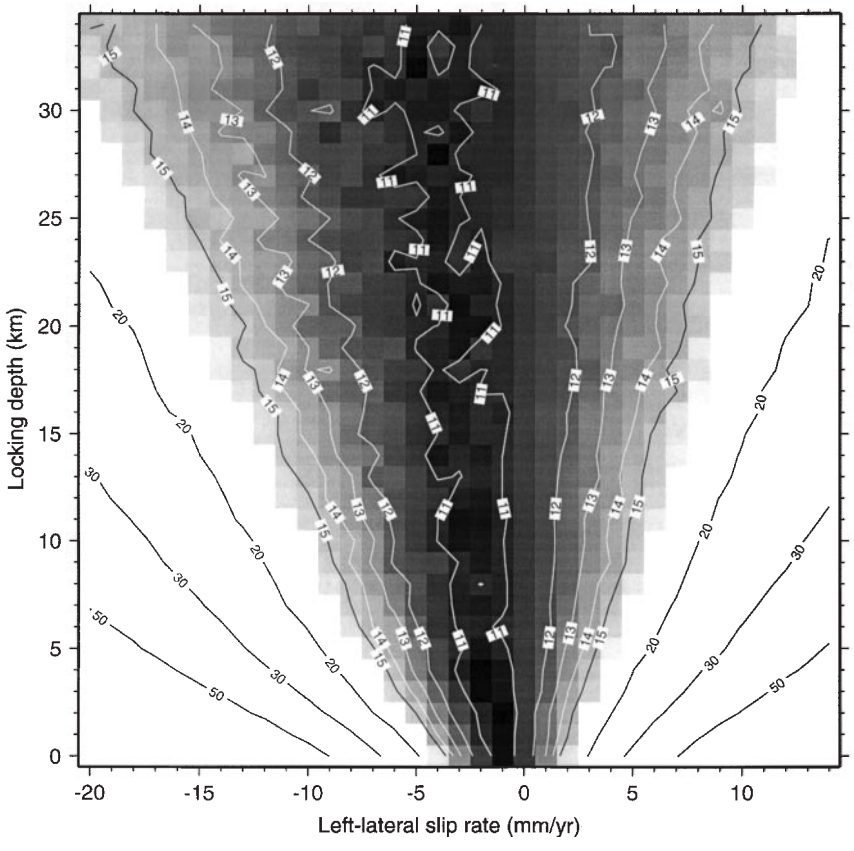

Fig. 7. Distribution of the χ^2 statistic for the residual (observed minus calculated) values of the 20 shear strain rates $\dot{\gamma}_1$ and $\dot{\gamma}_2$ as a function of two-dimensional model parameter space of locking depth D (in km) and the rate of left-lateral slip U_1 (in mm/year). The *shaded area* shows the region of 95% confidence for which $\chi^2 = 16.6$. The most likely values fall inside the innermost contour where $\chi^2 = 11.0$ and the level of confidence is 23%

The benchmark at YEN may have been disturbed between measurements by a local farmer. Stations DAU, NLA, and NNA were measured only twice.

As an additional quality control on the measured angles, we plot their rate of change in Fig. 4. Following Snay (1986), we write the rate of angular change normalized by $\sin\alpha$ as

$$(\Delta\alpha_i/\Delta t_i)\text{cosec}\ \alpha_i = \dot{\gamma}_{\max}\ \sin\ 2(\psi - \bar{\theta}_i) \qquad (6)$$

where α_i is the ith measured angle, ψ is the azimuth of $\gamma_{\max}$ and $\bar{\theta}_i$ is the azimuth which bisects the angle α_i. This expression corrects a minor error in Snay (1986). Such a plot highlights the "outlier" measurements excluded from the three-epoch inversion.

4 Estimation strategy

To estimate deformation parameters, we use the network adjustment software developed by Danan Dong (Dong 1993; Dong et al. 1998). This software has been applied to similar data sets in California (Bawden et al. 1997) and France (Ferhat et al. 1998).

Our data suffice to determine only the rates of horizontal angular shear $\dot{\gamma}_1$ and $\dot{\gamma}_2$ (Bibby 1982; Feigl et al. 1990). In other words, the rates of dilatation and rotation are undetermined. Similarly, without repeated leveling data, we must assume no vertical motion by fixing the elevation of each site to its GPS-derived value.

For clarity, we divide the network into triangular subnetworks, forming a Delaunay triangulation (Gold 1975; Watson 1982). Within each triangle, we estimate the angular shear rate parameters $\dot{\gamma}_1$ and $\dot{\gamma}_2$, which we assume to be constant in time.

To evaluate the sensitivity of the estimated strain rates to various corrections to the data set, we perform a suite of network adjustments, as follows:

1. Combination of direction lists from 1963 and 1983 with the full covariance matrix for the 1994 GPS solution.
2. Combination of direction lists from 1963, 1983, and 1994.
3. Combination of unreduced direction list with tie corrections from 1983.
4. Combination of reduced direction list without tie corrections from 1983.
5. With a correction for deflection of the vertical, assumed constant in time.
6. Without correction for deflection of the vertical.
7. With an artificial 10-m perturbation in the ellipsoidal height of a single station.

None of these perturbations alters the estimated values of $\dot{\gamma}_1$ and $\dot{\gamma}_2$ by more than one third of their uncertainties. We therefore conclude that they are fairly robust and use three direction lists (option 2) without any correction for deflection of the vertical (option 6) as input data for network adjustment.

Since the adjustment software parameterizes deformation in terms of station velocities, we must decide if and how to regularize the solution. There exist at least four options, as follows:

1. Free network, i.e. no constraints.
2. Minimum constraints, i.e. two fixed stations.
3. Inner coordinate solution (Segall and Matthews 1988).
4. Outer coordinate solution (Prescott 1981).

Once again, the estimated values of $\dot{\gamma}_1$ and $\dot{\gamma}_2$ do not change by more than one third of their uncertainties between the estimation strategies. This is to be expected, since the shear strain rates are invariant to changes in network scale and orientation, the same parameters which regularization strategies 2, 3, and 4 constrain. Henceforth, the "free-network" solution (regularization 1) will form the basis of our geophysical interpretation.

Results

The average strain rates estimated from the three-epoch 1963–1983–1994 data set for the whole network are $\dot{\gamma}_1 = -0.019 \pm 0.055\,\mu\text{rad/year}$ and $\dot{\gamma}_2 = -0.094 \pm 0.060\,\mu\text{rad/year}$. Considering subnetworks, we estimate the shear strain rates $\dot{\gamma}_1$ and $\dot{\gamma}_2$ in ten Delaunay triangles as a function of distance from the fault (Fig. 5). None of them are distinguishable from zero (no deformation) with 95% confidence. The measurements are not precise enough to detect a statistically significant geodetic signal from movement on the fault.

Figure 6 shows the same solution in terms of the maximum strain rate $\dot{\gamma}_{\max}$ and its azimuth ψ on a map with the Delaunay triangulation.

Nonetheless, we can interpret the observed strain rates in terms of the fault's activity. For example, the $\dot{\gamma}_1$ shear strain rate is positive in seven of the ten triangles, a result which is compatible with dextral simple shear on the NW-striking Red River fault system. Similarly, the azimuth ψ of maximum shear is parallel to the NW–SE trend of the fault, particularly in the three triangles near the Song Hong fault strand (Fig. 6). We interpret these results as interseismic deformation because no earthquake with magnitude larger than 5 has occurred within the geodetic network over the three decades spanned by the geodetic measurements (1963–1994).

The results for $\dot{\gamma}_2$ are more challenging to interpret. In terms of "pure" shear oriented NW–SE (perpendicular to the fault trace), we can interpret a positive value of $\dot{\gamma}_2$ as extension (indicative of normal faulting) and a negative value as compression (thrust faulting and/or folding). Both mechanisms are capable of producing topographic relief, as observed between the Song Chay and Tam Dao fault strands (near NLA at 0 km in the profile of Fig. 5). In this area, two of the four triangles show positive values of $\dot{\gamma}_2$. Consequently, we are unable to resolve the debate bettween fault-normal extension, as suggested by the triangular-faceted geomorphology of the Tam Dao fault above Tuyen Quang (Lacassin, pers. comm. 1994) and fault-normal compression, as indicated

by the two-epoch GPS results between the far-field GEODYSSEA sites NON and CAM (Walpersdorf 1997).

To further the interpretation, we apply a simple elastic dislocation model (Okada 1985; Feigl and Dupré 1996). Given the fault geometry, this model calculates the deformation field at the Earth's surface. We consider the special case of a vertical strike-slip fault locked at depth, as for the San Andreas fault in California (Savage 1990). To fit the observations, we vary two parameters in the fault model: the locking depth D (in km) and the rate of left-lateral slip U_1 (in mm/year). We evaluate the goodness of fit by calculating the χ^2 statistic for the residual (observed minus calculated) values of the 20 shear strain rates $\dot{\gamma}_1$ and $\dot{\gamma}_2$. A grid search over a reasonable portion of this two-dimensional parameter space shows that the optimal solution is not unique (Fig. 7). Indeed, the region of 95% confidence is too large to provide much new, useful information on the activity of the fault.

We can, however, limit the extent of the parameter space with external information on the locking depth of the fault. We can exclude small values, say $D < 5$ km, because they imply a fault creeping near the surface, which has not been observed in concrete structures crossing the fault trace. Similarly, we can exclude large values, say $D > 20$ km, because most of the earthquakes in the study area have hypocentral depths around 15 km (Fig. 1). Even if these depths are poorly determined, it seems unlikely that the seismogenic layer (which we mimic as the locked portion of the fault) is thicker than 20 km. By limiting our attention to the portion of the parameter space where the locking depth D is between 5 and 20 km, the most likely values for the deep slip rate U_1 are between 1 and 5 mm/year of right-lateral motion. These values fall within the contour for 23% confidence. At 95% confidence, the slip rate should fall between 7 mm/year of left-lateral motion and 15 mm/year of right-lateral motion.

6 Conclusion

We have used a time series of geodetic observations at three distinct epochs over 31 years in a network spanning an active fault. The imprecision of the early triangulation measurements limits our ability to make hard conclusions. At the level of 95% confidence, we detect no significant deformation in the network. Nonetheless, the estimated rates of shear strain rate favor the following points in a geophysical interpretation.

1. The Red River Fault system is most likely to be active in the present day as a right-lateral strike-slip fault. This result is consistent with a change in the sense of the fault slip sometime after 5 Ma ago, as most recently argued by Leloup et al. (1995).
2. The amount of slip at depth, below a currently locked seismogenic layer, is likely to be between 1 and 5 mm/year. In the absence of any aseismic "creeping" deformation, this rate should correspond to the "long-term" Plio-Quaternary slip rate for the Red River fault system in norhtern Vietnam, in approximate agreement with an independent estimate of the order of 5 mm/year based on a geomorphologic analysis of offsets in the drainage system by the same fault system in Yunnan, south China (Replumaz and Lacassin 1977).
3. The geodetic data are not precise enough to resolve any motion perpendicular to the fault to within about 0.2 μrad/year. The question of whether the fault system presently has a component of extensive or compressive motion remains open.

A second GPS survey before the year 2000, repeating the 1994 campaign, will decrease the uncertainty on the rates of deformation. It will also yield the vector velocity field, rather than just the rates of angular shear strain.

Acknowledgments. The authors are grateful to Professors Paul Tapponnier and Nguyen Trong Yem for inspiring this work. They thank Danan Dong for supporting his adjustment software and patiently answering many questions. Nguyen Hong Phuong of the Seismological Laboratory of Hanoi Branch – Institute of Oceanography. NCNST of Vietnam generously provided the earthquake catalogue. Robin Lacassin and Alexis Rigo commented helpfully on the manuscript and Andrea Walpersdorf kindly provided her results in advance of publication. Gilles Peltzer contributed critical insights to the field reconnaissance. The authors thank their colleagues from Toulouse and Hanoi for stalwart assistance in the field: Doan Van Tuyen, Erik Doerflinger, Do Minh Kien, Gilbert Ferhat, Pierre Genthon, Hoang Quang Vinh, Marc Monnereau, Ngo Quoc Dung, Nguyen Quang Xuyen, Nguyen Viet Ninh, Mai Thanh Tan, Pham Tich Xuan, Phan Trong Trinh, Matthieu Sylvander, Tran Canh, Tran Dinh To, and Tran Van Doan. The triangulation data were collected from the Center of Information and Documentation of Geodetic Survey of Vietnam. All figures were produced with the public-domain GMT software (Wessel and Smith, 1991). This study was supported by a fellowship from the French Ministry of Foreign Affairs and a grant from CNRS/INSU Programme Tectoscope–Positionnement.

References

Allen CR, Gillespie AR, Han Yuan, Sieh KE, Zhang Buchum, Zhu Chengnan (1984) Red River and associated faults, Yunnan Province, China. Quaternary geology, slip rates and seismic hazard, Bull Geol Soc Am 95: 686–700

Armijo R, Tapponnier P, Tonglin H (1989) Late Cenozoic right-lateral strike-slip faulting in Southern Tibet. J Geophys Res 94: 2787–2838

Bawden GW, Donnellan A, Kellogg LH, Dong D, Rundle JB (1997) Geodetic measurements of horizontal strain near the White Wolf fault, Kern County, California, 1926–1993. J Geophys Res 102: 4957–4975

Beutler G, Brockmann E, Gurtner W, Hugentobler U, Mervart L Rothacher M, Verdun A (1994) Extended orbit modeling techniques at the CODE Processing Center of the International GPS Service for Geodynamics (IGS): theory and initial results. Manuscr Geod 19: 367

Bibby HM (1982) Unbiased estimate of strain from triangulation data using the method of simultaneous reduction. Tectonophysics 82: 161–174

Bomford G (1980) Geodesy, 4th edn. Clarendon Press, Oxford, 855 pp

Boucher C, Altamimi Z, Feissel M, Sillard P (1996) Results and analysis of the ITRF94, IERS Tech note 20, Observatoire de Paris

Briais A, Patriat P, Tapponnier P (1993) Updated interpretation of magnetic anomalies and seafloor spreading stages in the South China Sea: implications for the Tertiary tectonics of Asia. J Geophys Res 98: 6299–6328

Dong D (1993) The horizontal velocity field in Southern California from a combination of terrestrial and space-geodetic data. Ph.D. thesis, Mass. Inst. Tech. Cambridge, 157 pp, 1993

Dong D, Herring TA, King RW (1998) Estimating regional deformation from a combination of space and terrestrial geodetic data. J Geod 72: 200–214

Duong CC, Feigl K, Nguyen Trong Yem, Tran Dinh To, Phan Trong Trinh, Peltzer G, Lacassin R, Tapponnier P, Dang Hung Vo, Tran Vinh Lu (1994) Terrestrial surveying measurements of deformation across the Red River Fault near Thac Ba, Vietnam, 1963–1983. In: Int Workshop Seismotectonics and Seismic Hazard in South East Asia, Hanoi pp 34–39

Duquesnoy T, Barrier E, Kasser M, Aurelio M, Gaulon R, Punongbayan RS, Rangin C French-Philipine Cooperation Team (1994) Detection of creep along the Philippine fault: first results of geodetic measurements on Leyte island, central Philippine. Geophys Res Lett 21: 975–978

Feigl KL, Dupré E (1996) RNGCHN: a program to calculate displacement components from dislocatioin in an elastic halfspace with applications for modleing geodetic measurements of crustal deformation (ftt://spike.cst.cnes.fr/pub/GRGS/rngchn.tar.Z). Comput Geosci (in press)

Feigl KL, King RW, Jordan TH (1990) Geodetic measurement of tectonic deformation in the Santa Maria fold and thrust belt, California. J Geophys Res 95: 2679–2699

Feigl KL Agnew DC, Bock Y, Dong D, Donnellan A, Hager BH, Herring TA Jackson DD, Jordan TH, King RW, Larsen S, Larson KM, Murray MH, Zhengkang Shen, Webb FH (1993) Space geodetic measurement of crustal deformation in central and southern California, 1984–1992. J Geophys Res 98: 21 677–21 712

Ferhat G, Feigl KL, Ritz JF, Souriau A (1998) Geodettic measurement of tectonic deformation in the Southern Alps and Provence, France, 1947– 1994. Earth Planet Sci Lett 159: 35–46

Frank FC, (1966) Deduction of earth strains from survey data. Bull Seism Soc Am 56: 35–42

Gold CM (1975) Automated contour mapping using triangular element data structures and an interpolant over each irregular domain. Comput Graph 11: 170–175

Herring TA (1995) Global Kalman Filter VLBI and GPS analysis program, version 4.0. Massachusetts Inst Technol, Cambridge

Jaeger JC, Cook NGW (1979) Fundamentals of rock mechanics. Chapman &Hall, London, 593 pp

King RW, Bock Y (1995) Documentation for the GAMIT GPS analysis software, release 9.32. Massachusetts Inst Technol, Cambridge

Lacassin R, Leloup PH, Tapponnier P (1993) Bounds on strain in large Tertiary shear zones of SE Asia from boundinage restoration. J Struct Geol 15: 677–692

Lacassin R, Tapponnier P, Leloup HP, Phan Trong Trinh, Nguyen Trong Yem (1994) Morphotectonic evidence for active movements along the Red River Fault Zone. In: Int Workshop Seismotectonics and Seismic Hazard in South East Asia. Hanoi, pp 66–71

Leloup PH, Lacassin R, Tapponnier P, Schärer U, Zhong Dalai, Liu Xiaohan, Zhang Liangshang, Ji Shaocheng, Phan Trong, Trinh (1995) The Ailao Shan–Red River shear zone (Yunnan, China), Tertiary transform boundary of Indochina. Tectonophysics 251: 3–84

Malvern LE (1969) Introduction to the mechanics of a continuous medium. Prentice-Hall, Englewood Cliffs, NJ, 713 pp

Molnar P, Gipson JM (1996) A bound on the rheology of continental lithosphere using very long baseline interferometry: the velocity of south China with respect to Eurasia. J Geophys Res 101: 545–553

Molnar P, Tapponnier P (1975) Cenozoic tectonics of Asia: effects of a continental collision. Science 189: 419–426

Okada Y (1985) Surface deformation due to shear and tensile faults in a half-space. Bull Seism Soc Am 75: 1135–1154

Peltzer G, Saucier F (1996) Present-day kinematics of Asia derived from geologic fault rates. J Geophys Res 101: 27 943–27 956

Prescott WH (1976) An extension of Frank's method for obtaining crustal shear strains from survey data. Bull Seism Soc Am 66: 1847–1853

Prescott WH (1981) The determination of displacement fields from geodetic data long a strike slip fault. J Geophys Res 86: 6067–6072

Prescott WH, Savage JC, Kinoshita WT (1979) Strain accumulation rates in the western United States between 1970 and 1978. J Geophys Res 84: 5423–5435

Replumaz A, Lacassin R (1997) Plio-Quaternary slip rate along the active Red River fault deduced from long term river offsets. Terra Nova 9 (Abstr Suppl 1): 239

Rothacher M, Beutler G, Brockmann E, Mervart L, Schaer S, Springer TA, Wild U, Wiget A, Boucher C, Seeger H (1996) Annual report 1995 of the CODE analysis center of the IGS. IGS 1995 Ann Rep Pasadena pp 151–186

Savage JC (1990) Equivalent strike-slip earthquake cycles in halfspace and lithosphere–asthenosphere Earth models. J Geophys Res 95: 4873– 4879

Savage JC, Burford RO (1970) Accumulation of tectonic strain in California. Bull Seism Soc Am 60: 1877–1896

Segall P, Matthews MV (1988) Displacement calculations from geodetic data nd the testing of geophysical deformation models. J Geophys Res 93: 14 954–14 966

Snay RA (1986) Horizontal deformation in New York and Connecticut: examining contradictory results from the geodetic evidence. J Geophys Res 91: 12 695–12 702

Tapponnier P, Peltzer G, Le Dain AY, Armijo R, Cobbold P (1982) Propagating extrusion tectonics in Asia: new insights from simple experiments with plasticine. Geology 10: 611–616

Tapponnier P, Laccassin R, Leloup PH, Schärer U, Zhong Dalai, Liu Xiaohan, Shaocheng J, Zhang Lianshang, Zhong Jiayou (1990) The Ailao Shan/Red River metamorphic belt: Tertiary left-lateral shear between Indochina and China. Nature 343: 431–437

Vanícek P, Krakiwsky EJ (1986) Geodesy: The concepts, 2nd edn North- Holland, Amsterdam, 697 pp

Walpersdorf A (1997) L'observation de la tectonique active en Asia du Sud-Est par géodésie spatiale: un project GPS, Doctoral Thesis, Ecole Normale Supérieure, Paris

Watson DF (1982) ACORD: automatic contouring of raw data. Comput Geosci 8: 97–101

Weldon R, Sieh K, Zhu O, Han Y, Yang J, Robinson S (1994) Slip rate and recurrence interval of earthquakes on the Hong He (Red River) fault, Yunnan, PRC. In: Int Workshop Seismotectonics and Seismic Hazard in South East Asia, Hanoi pp 244–248

Wessel P, Smith WHF (1991) Free software helps map and display data. EOS. Trans Am Geophys union 72(41): 441